Biosensors and Bioelectronics 96 (2017) 17–25

Contents lists available at ScienceDirect

Biosensors and Bioelectronics

journal homepage: www.elsevier.com/locate/bios

Recent progress in Prussian blue films: Methods used to control regular nanostructures for electrochemical biosensing applications

Zhenyu Chu, Yu Liu, Wanqin Jin*

State Key Laboratory of Materials-Oriented Chemical Engineering, Jiangsu National Synergetic Innovation Center for Advanced Materials, College of Chemical Engineering, Nanjing Tech University, 5 Xinmofan Road, Nanjing 210009, PR China

ARTICLE INFO

Keywords:
Prussian blue
Regular nanostructures
Nanocontrol methods
Biosensors
Performance enhancement

ABSTRACT

In the last decade, Prussian blue (PB) has attracted increased scientific interest in various research fields, such as fuel cells, gas separation and pollution treatment. Due to its advanced catalysis, biocompatibility, selectivity and stability, PB has been widely used in biosensor construction. However, the formation of regular PB nanostructures is challenging due to its fast crystallization rate. Recently, developments in this research area have increased due to emerging novel synthesis methods in nanoscale technology. Various regular nanostructures of PB films that show superior biosensing performance have been prepared. In this review, recent research progress in PB nanostructures is summarized, with special emphasis on the methodology of nanostructure control. The mechanism and key factors in regular PB crystallization are also discussed for each synthesis method. The performance of PB nanostructure-based biosensors is compared with others to show the advantages of nanostructure control. The methodology discussed in this review not only include the regular growth of PB films, but also provides information on the nanostructure control of more crystalline materials, including PB analogues, noble metals, metal oxides and coordination compounds. In addition to biosensing applications and the development of more advanced nanostructures, PB has also shown increased advanced properties in other scientific areas.

1. Introduction

Prussian blue (PB), which is a typical hexacyanoferrate coordination compound (Fig. 1a), has attracted considerable attention in various scientific fields due to its unique properties (Ferlay et al., 1995; Karyakin et al., 1995; Buser et al., 1977; Lu et al., 2012). It was first synthesized for use as a dark blue pigment (Fig. 1b) by the German paint maker Diesbach in 1704 (Holtzman, 1945). This material has a face-centered cubic structure of the unit cell, the ideal edge length of the cell lattice is 10.143 Å and is composed of only three elements: iron, carbon and nitrogen (Itaya et al., 1986; Herren et al., 1980). Due to its cell structure and composition, it was known as a simple metal organic frameworks (MOFs) material by some researchers (Okubo et al., 2010; Xiao et al., 2015), but it is much more stable than MOFs, especially in water.

Interestingly, each neighboring iron in PB has two different valances, Fe(II) and Fe(III), for building the skeleton with the CN group. Every adjacent twelve Fe-CN-Fe edges of the unit cell can construct a large cavity which allows the entrance of alkali metal ions, such as Na^+ and K^+, to increase conductivity (Bleuzen et al., 2004; Karyakin, 2001; Crumbliss et al., 1984). Its standard chemical formula is $Fe_4[Fe(CN)_6]_3$, and the Fe(II) is hex-coordinated with CN and then combined with Fe(III). In addition to its nontoxicity and biocompatibility, PB can be easily excited to induce its catalytic function due to its low energy gap (Yamamoto et al., 2009). All the above characteristics provide the electrocatalytic function of PB which has been widely employed as an electrode material since 1978 (Neff et al., 1978; Karyakin et al., 1995; Ricci and Palleschi, 2005).

PB is a highly efficient electrode modifier in biosensor fabrication. To date, numerous researchers have adopted this material for the detection of various physiological activators (Haghighi et al., 2010). Since 1978, more than 2000 papers have been published in this field. From 2010 to now, more than 1110 of these papers have shown interest in the development of PB-based biosensors. However, with the development of nanoscience, a vital disadvantage of PB has been exposed, which is an obstacle in the further improvement of sensing performance. This disadvantage is control of the PB nanostructure. Traditional synthesis of PB mainly depends on the chemical reaction between ferrocyanide and iron ion (Coleby, 1939). Although this method results in the rapid preparation of PB, the obtained crystal

* Corresponding author.
E-mail address: wqjin@njtech.edu.cn (W. Jin).

http://dx.doi.org/10.1016/j.bios.2017.04.036
Received 11 January 2017; Received in revised form 7 April 2017; Accepted 25 April 2017
Available online 26 April 2017
0956-5663/

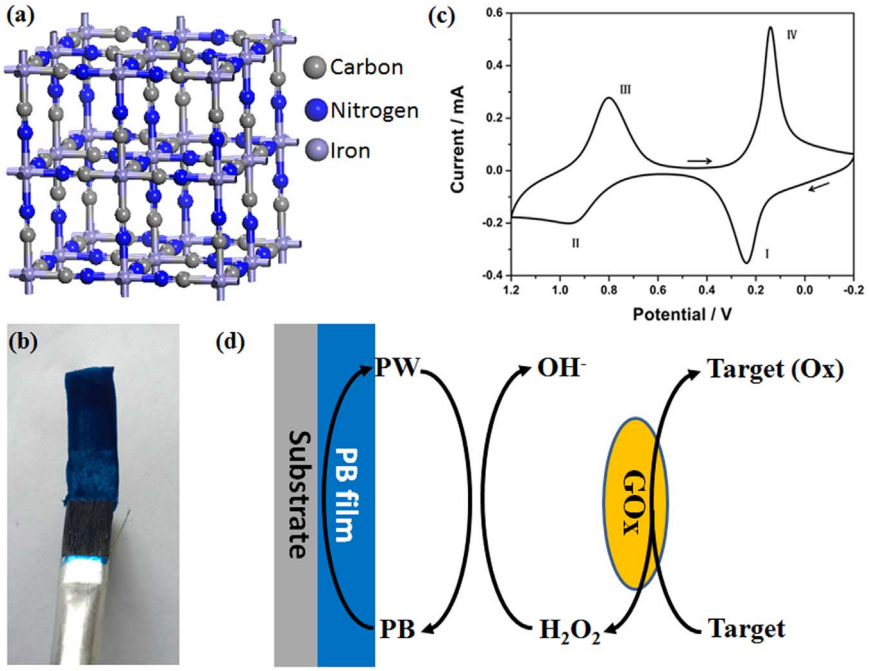

Fig. 1. (a) Unit cell structure of PB; (b) Digital photo of painted PB ink; (c) CV diagram of PB modified Pt electrode in 0.1 M PBS with 50 mV/s scanning rate; (d) Mechanism of PB-based biosensor.

structure is always irregular, which may strongly affect the catalytic ability of the prepared biosensor. Therefore, in recent years, PB research has mainly focused on the development of methodology for nanostructure control (Puganova and Karyakin, 2005; Gimenez-Romero et al., 2007; Zhang et al., 2013). Various novel preparation strategies have been designed to synthesize regular PB crystals, and more importantly, these special nanostructures have been confirmed to possess stronger electrocatalysis and conductivity, which obviously improve the biosensing performance of PB films (Chu et al., 2011; Du et al., 2010; McHale et al., 2010; Roy et al., 2011). Moreover, PB is an important metal coordination compound with numerous family analogues (Tang et al., 2016; Kaye and Long, 2005; Aguila et al., 2016). The two Fe sites can both be changed to different metals (such as Co, Ni, Mn, Cr), and the CN group can be replaced by other organic groups. This type of compound has a multiple element composition and shows various characteristics, but retains the same cell structure (Han et al., 2016; Jiang et al., 2016). Therefore, understanding its growth behavior, electrochemical features and nanostructure control technologies is meaningful and beneficial in identifying more analogue materials and their nanostructures in the fabrication of new biosensors.

In this review, we will describe the mechanisms of PB-based electrochemical biosensors, introduce traditional preparation methods (such as chemical synthesis and electrodeposition methods) and their development history, and discuss the disadvantages of PB nanostructure control. Emphasis is given to the novel developed approaches for the successful production of various nanostructures, and the principles of crystallization control will be discussed to provide guidance on material synthesis. Finally, the advantages of these regular PB nanostructures and their applications in various biosensors are discussed. Using this approach, we hope to provide an overview of recent progress in PB nanostructure synthesis and the wide application of PB in electrochemical biosensors. A summary of nanocontrol methodology may provide new motivation for the development of other useful nanostructures of PB and its analogues.

2. Electrochemical behavior of PB

The electrochemical properties of PB are mainly derived from the iron elements. Due to the two different valances of iron in its unit cell, PB can produce electron movement for easy oxidation or reduction by the external potential. There are three common forms of PB with different valances: further oxidation of all Fe(II) to Fe(III) is called Berlin Green (BG); mixed coexistence of Fe(II) and Fe(III) is PB; transformation of all Fe(III) to Fe(II) can produce Prussian White (PW) (Liu et al., 2009a, 2009b; Zhang et al., 2016; Sgobbi et al., 2016). Normally, this behavior can be expressed by the cyclic voltammetry (CV) diagram of PB (Fig. 1c). The pair of redox peaks I and IV describe the change between PB and PW, and II and III represent the conversion between PB and BG. Normally, because the synthesis sources of PB contain alkali metal ions such as K^+ or Na^+, the prepared PB which has the ions in its lattice can show weak solubility (Doumic et al., 2016; Manivannan et al., 2016).

The electrochemical activity of PB was demonstrated to rely on the existence of alkali metal ions in the PB lattice (Du et al., 2016; Itaya et al., 1982). Researchers believe the electrochemical reaction of PB is always related to the quantitative change in alkali metal ions. However, to date, there has been no definite clarification of its redox mechanism. However, the electrocatalytic principle has been generally accepted. Accompanying the transformation from PW to PB, H_2O_2 can be quickly reduced to OH^- by the transferred electrons, and PB can again be reduced to PW under an appropriate potential (Qiu et al., 2007b). During this process, PB acts as the electron carrier to transport electrons from the electrode surface to H_2O_2. Due to the excellent electrocatalysis of H_2O_2, PB is known as the "artificial peroxidase" (Karyakin et al., 2000). In addition, because H_2O_2 is one product of most oxidase reactions, PB can be employed as the core biosensor material in the detection of various physiological activators (Fig. 1d), such as glucose, lactate and glutamate (Y Jiang et al., 2016; D Jiang et al., 2016; Xu et al., 2015; Imani et al., 2016; Salazar et al., 2016). PB has very low operation potential, normally lower than 0 V (*vs.* Ag/AgCl). Therefore, PB-based biosensors can possess excellent anti-interference ability regarding other co-existing substances in blood or serum, such as ascorbic acid and uric acid.

According to the band structure of PB, the band gap between the highest occupied molecular orbital (HOMO) and the lowest unoccupied molecular orbital (LUMO) is approximately 1.43 eV which belongs to

the semiconductor (Chu et al., 2010). Hence, electron transfer resistance is the main problem in electrocatalytic performance. However, a number of reports have confirmed that not only electrocatalysis but also resistance are definitely associated with the nanostructure of PB. Using the same scanning parameters, ΔE (potential difference between the reduction and oxidation peaks) of the PB film can shift from 0.1 to 0.2 mV with changing structures (Liu et al., 2009a, 2009b; Lu et al., 2013). A dense film with fewer disadvantages is often beneficial in decreasing electron transfer resistance. In contrast, regular PB crystals that have high electrocatalysis cannot form dense films due to the geometric stack. This trade-off between electrocatalysis and resistance has always existed in the application of PB films. Therefore, selection of the synthesis method on the PB nanostructure is essential for biosensing performance.

3. Traditional preparation methods for PB films

The use of PB normally requires the formation of a modified film on the electrode surface. The first synthesis of PB was based on a chemical reaction between potash and animal blood (Ware, 2008). To date, this method is still the fastest way of obtaining PB films. For a long time, PB has been used as a pigment for paints without an extensive study of its properties. Since the concept of "chemically modified electrode" was proposed by Murray in 1975 (Murray, 1980), a PB film-modified electrode was first prepared by Neff in the 1980s (Neff, 1978; Ellis et al., 1981). He named this preparation method the electrochemical deposition approach. The above two methods are the most commonly used strategies in PB film preparation, and with continuous development, they have also evolved to produce lots of different forms. Electrochemical deposition is normally used in the *in-situ* synthesis of PB on the electrode, and the chemical reaction method often focuses on the formation reaction of PB before adhesion on the electrode.

3.1. Chemical reaction method

The chemical reaction method for PB film synthesis is mainly due to the reaction between $[Fe(CN)_6]^{4-}$ and Fe^{3+} ions, and the reaction equation is:

$$3A_4Fe(CN)_6 + 4FeB_3 \rightarrow Fe_4[Fe(CN)_6]_3 + 12\ AB \quad (1)$$

Here, A represents the alkali metal ion, and B is the matching anion. Ricci et al. (2003) dipped the screen-printed electrode into the acid reaction solution which was a mixture of $K_3Fe(CN)_6$ and $FeCl_3$ reactants at a 1:1 concentration ratio for a preparation time of 1 h, and then dried at 100 °C to finish. This PB film has excellent pH tolerance to weak alkaline conditions of pH=9 (normally PB can only exist in an acid and neutral environment). Zakharchuk et al. (1995) used a mechanical process, the abrasive transfer technique, to immobilize PB slurry which was synthesized by the chemical reaction method on a carbon paste electrode for PB film preparation. This research demonstrated that the PB film exhibited a pronounced proton exchange property with a reversible electrochemical behavior. Other studies on the chemical synthesis of PB films are similar to the above two methods, and some modification and development are necessary to improve the performance of the PB film, such as a change in the immobilization method and the use of cross-linkers on the substrate (Shen et al., 2009; Guo et al., 1999).

Currently, there are only a few studies that have adopted the chemical reaction method to prepare PB films for biosensor application. Although this method can quickly produce a large amount of PB, it does not control the nanostructure of the synthesized PB with satisfactory reproducibility. Moreover, the *ex-situ* preparation often demands the assistance of sticky cross-linkers which increase the interface resistance to decrease the efficiency of electron transfer.

3.2. Electrochemical deposition method

Electrochemical deposition is the most frequently used technology for PB film preparation. It works by using certain cycle potentials on the electrode to drive the reduction or oxidation of the electroactive target on the supporting electrode for film formation. In the literature, electrochemical deposition mainly consists of three strategies: constant current, constant potential and CV scanning processes. The first adoption of this approach for PB film preparation was performed in 1978. Neff (1978) imposed a constant current of 1 mA on a platinum foil which was immersed in a reactive solution prepared using an equal amount of 0.01 M $FeCl_3$ and $K_4[Fe(CN)_6]$ with 1 M HCl for 1 h to allow deposition. This electrode was the first electrodeposited PB film, and inspired by this work, numerous modified electrochemical deposition approaches have been developed. Subsequently, Itaya et al. (1986) dipped a cathodically polarized electrode into a mixture of ferric ferricyanide solution for PB film preparation. He proposed that the supporting electrode material had a big influence on the electrodeposition effects. Organic substrates cannot be used in electrochemical deposition due to rapid cover of PB on the electrode surface with very poor adherence during oxidation of the PB film. Karyakin et al. (1999) used a constant 0.4 V for the preparation of a PB film, and obtained a highly sensitive PB biosensor after 60 s deposition. This study demonstrated that PB can maintain stability under negative potential with neutral supporting electrolyte solutions. In addition, this group used CV scanning between −0.1 and 0.5 V to modify PB on a glassy carbon electrode using redox processes (Karyakin et al., 2007). After 10 min deposition, an integrated PB film was prepared which showed good selectivity due to the low operation potential. As reported, the selection of a supporting electrolyte can strongly affect the behavior of electrodeposition (Abbaspour and Kamyabi, 2005). Various electrolyte solutions of alkali metal salts (KCl, K_2SO_4, KNO_3, KF, $KClO_4$, K_2CO_3 NH_4NO_3, $CsNO_3$ and $RbNO_3$) were tried to mix with the deposition solution. The results demonstrated that KCl promoted the deposition efficiency under a very low potential range using CV scanning. Interestingly, by using KCl as the electrodeposition electrolyte, PB can be synthesized in only single $K_4[Fe(CN)_6]$ solution due to the decomposition of $K_4[Fe(CN)_6]$ in the electrochemical environment.

To date, electrochemical deposition is still a highly efficient method for *in-situ* preparation of PB films. However, it is not useful in controlling the PB nanostructure due to the rapid preparation process. Moreover, this method strongly relies on the material and roughness of the substrate. An uneven electrode surface can induce over-accumulation of crystals at the partial sites to produce an unbalanced distribution which can cause an increase in electron transfer resistance and a decrease in catalytic area. Therefore, with the aim of performance enhancement, the development of novel techniques is expected for the creation of PB film nanostructures.

4. Novel preparation methods for PB films

The principle of crystallography results in the initial formation of seeds, and further growth relies on these seeds acting as the cores for accumulation. The reason for hard control of the PB nanostructure using the above two methods is attributed to their rapid crystallization speeds, which tend to produce mass seeds with a tight distribution on the support. This hinders sufficient growth of a single crystal and does not form a regular nanostructure due to space constraints. Accordingly, the key to realizing regular synthesis of the PB film is to control seed formation.

Based on the above principle, self-assembly, the template-assisted method, hydrothermal synthesis and many other approaches have been developed. The following description will provide an introduction and analysis of these methods and the various nanostructures of PB films, and a discussion on the control mechanisms in nanostructure formation. Critical factors for the regular growth of PB films will also be

discussed to benefit the further design of novel strategies.

4.1. Self-assembly method

Preparation of PB films by the self-assembly method was initially developed in 2001 (Millward et al., 2001). In this method, a layer of cationic polyelectrolyte was first modified on the supporting electrode to show a positive charge. This charged electrode was initially dipped into $[Fe(CN)_6]^{4-}$ solution to adhere the anions by electrostatic interaction. The electrode was then dipped into Fe^{3+} solution to produce the reaction and form the PB film. The above dipping steps can be repeated to adjust the coverage and thickness of the PB film. The outcome of this method is the result of the principle of layer upon layer, which is supposed to qualify structure control. However, during this period, the nanostructure of PB is not well controlled and a regular crystal shape is not formed. Since 2009, we have carefully studied the self-assembly process to clarify the influence of various preparation parameters on PB structure (Liu et al., 2009a, 2009b). A decrease in pH value and increase in K^+ electrolyte concentration during preparation was confirmed to benefit the formation of smaller PB particles with a more uniform distribution. Importantly, the presence of polyelectrolyte modified before assembly was confirmed as the main obstacle in regular growth of the PB film. This polymer layer has high viscosity with numerous positive charges to rapidly catch the $[Fe(CN)_6]^{4-}$ ions on its surface. The characteristics of this first layer affect PB film formation. Therefore, we investigated the relationships between the modification conditions of polyelectrolyte (poly(diallyldimethylammonium chloride, PDDA as the sample)) and the morphology of the assembled PB film (Zhang et al., 2011). The results showed that the amount of PDDA loaded, which was controlled by the adsorption temperature, strongly affected the structure of the prepared PB crystals. The less PDDA deposited, more regular crystals were formed. Based on the above conclusion, we further attempted to directly use a bare electrode without polyelectrolyte modification to assemble the PB film (Liu et al., 2014). By controlling the deposition layers and temperature, numerous embedded PB nanocubes 100 nm in size were *in-situ* synthesized on a graphite electrode (Fig. 2). Due to the intergrowth of each crystal, the as-prepared PB film showed good continuity with few disadvantages, although most crystals only exposed a partial feature of the nanocube. It should be noted that the layer-by-layer method, which is similar to self-assembly, is often employed for the fabrication of composite PB films (DeLongchamp et al., 2004; Zhao et al., 2005). However, with this method it is difficult to achieve the regular growth of PB with other materials except before the synthesized regular crystals.

Self-assembly is an advanced method with high controllability for the formation of the PB nanostructure. Deposition temperature, cycle number and reactant concentration are the main parameters for adjusting the morphology of the prepared PB film. Nevertheless, the disadvantage of this approach is that it is time consuming. Normally, to obtain an integrated film, dozens of deposition cycles are required. Due to the easy self-reaction of acid ferrocyanide solution, fresh preparation is frequently performed to avoid this influence. Hence, waste increases as the number of cycles increase.

4.2. Template-assisted method

In nanoscience, nanostructure exploration using a template is a special method of nanoscale synthesis, where the structure of the target material is limited by or follows the adopted template (Xu et al., 2007; Li et al., 2013; Wang et al., 2008; Thomas et al., 2008). As previously mentioned, PB cannot spontaneously form a regular structure easily; therefore, the introduction of a template during PB preparation is a simple strategy to solve this problem. Anodic aluminum oxide (AAO) has been widely used as a hard template for the construction of tube or porous nanostructures (Routkevitch et al., 1996; Lee et al., 2014). Zhou et al. first synthesized a highly ordered porous alumina template with a hole size of 50 nm by a two-step anodizing method from a pure alumina foil (Zhou et al., 2002). The PB was then electrodeposited into the cavities of AAO. After removal of the template by 1 M H_2SO_4, integrated and ordered PB nanowires of 50 nm diameter were formed. In addition, using AAO, Johansson et al. developed a sequential deposition technique that relies on the alternate deposition of acid $K_4[Fe(CN)_6]$ and $FeCl_3$ solutions on the template (Fig. 3a) (Johansson et al., 2005). The authors found that the size and morphology of the prepared PB nanoparticles were related to the deposition times. After 10 cycles of deposition, nanocubic PB crystals that were free-standing without the support of the template were observed. Further adjustment of the template dimension could tailor the length and the outer as well as the inner diameter of the PB tubes.

Besides AAO, anodic titanium oxide (Gao et al., 2014), mesostructured silica (Goux et al., 2009) and carbon nanotube (Zhang et al., 2004a, 2004b) have also been used in the fabrication of PB nanostructures. The deposition methods of PB for these are similar with that used for AAO. These hard templates often require the strong acid to be removed, which may be dangerous for operators. Some soft templates usually consisting of polymers are easily erased by very mild conditions. Qiu et al. (2007b) adopted a multilayered polystyrene (PS) colloid as the template during the electrodeposition of PB. Tetrahydrofuran was only used for immersion, and a 3D ordered macroporous PB film was revealed on the ITO surface. We further extended this method using the mono-layer PS template (Fig. 3b) (Chu et al., 2012). The surfactant, sodium n-dodecyl sulfate, can induce mono-dispersion of PS beads. Using the self-assembly approach, PB filled the gap produced by the geometrical stack of neighboring beads to form a single layer of a PB nano-porous network after toluene

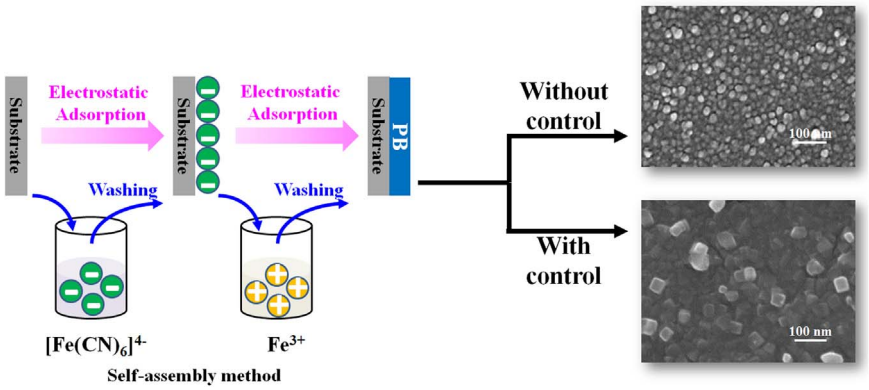

Fig. 2. Schematic of the self-assembly method for the synthesis of a PB nanocubes-based film. Reproduced from Liu et al. (2009a, 2009b) and Liu et al. (2014) with permission from Elsevier.

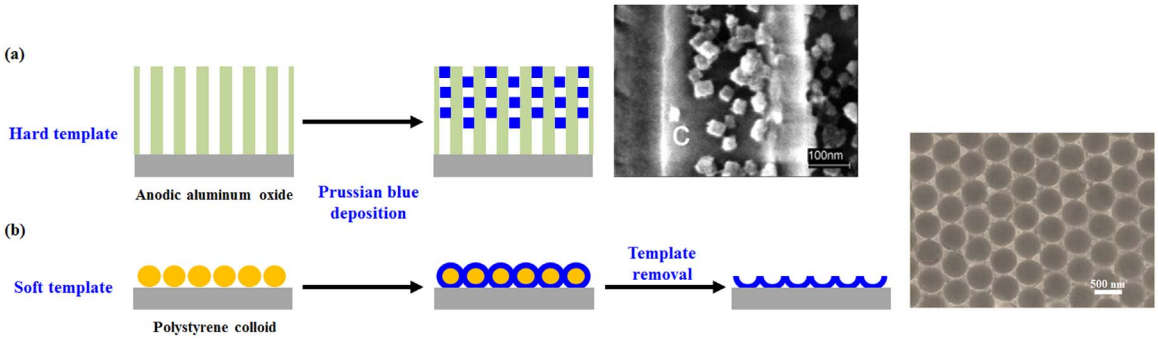

Fig. 3. Preparation routes using the template-assisted method for regular PB nanostructures with hard (a) and soft (b) templates. FESEM images in (a) and (b) show the prepared PB nanostructured film. Reproduced from Johansson et al. (2005) and Chu et al. (2012) with permission from American Chemical Society and Royal Society of Chemistry, respectively.

washing. Qu et al. found that the polycarbonate membrane induced the oriented growth of PB crystals to form a nanowire structure (Qu et al., 2007). Each PB nanowire was independent with a larger space between neighboring crystals than their diameter. The authors believed that this morphology can work as the performance of the numerous individual nano-electrodes was enhanced.

Silver (Ag) nanospheres and nanorods can also be used as templates for the construction of PB hollow nanostructures (Shen et al., 2014). After the formation of a nanostructured Ag suspension by thermal reduction, $K_3[Fe(CN)_6]$ and $Fe(NO_3)_3$ solutions were mixed to synthesize PB shells around the surface of Ag nanocrystals. This reaction relied on the consumption of Ag for the reduction of $K_3[Fe(CN)_6]$ to $K_4[Fe(CN)_6]$, which the authors called a sacrificial template method. With the continuous synthesis of PB, the Ag template was gradually reacted, which left the interior hollow. Based on the different morphologies of Ag nanospheres and nanorods, the PB shapes can be constructed as hollow nanospheres and nanotubes, respectively. These two types of PB nanocrystals were then immobilized on a GCE electrode to investigate their electrocatalysis. According to a comparison of CV results, the PB nanotube-based electrode exhibited higher electrocatalytic activity due to its 1D nanostructure and provided an easy and fast transfer tunnel for catalytic electrons. Although using this method can produce various PB nanostructures by following the adopted Ag morphologies, the Ag template cannot be totally erased.

The template-assisted approach is able to construct regular nanostructures using a feasible process. However, the extra introduction of material as a template also results in difficult removal. Although a soft template can be dissolved by some strong polar solvents, a few residues are not washed away, which could affect the performance of the PB film.

4.3. Hydrothermal synthesis method

For crystal cultivation, hydrothermal synthesis has been widely used in the growth of single crystals (Wang and Li, 2002a; Mo et al., 2002; Wang et al., 2002; Yu et al., 2013). However, this method is not promoted in the formation of nanostructured PB. This is probably due to its fast crystallization speed. The high temperature of the hydrothermal process can even accelerate the formation of PB crystals, which induces rapid accumulation and intergrowth. In 2003, Kitagawa et al. first found that the agglomeration process of PB can be controlled using appropriate protective polymers (Uemura and Kitagawa, 2003). Following this, some researchers reported their success in nanostructure control of PB crystals through various protectors using the hydrothermal strategy. Commonly used protectors are all polymers, such as polyvinylpyrrolidone (PVP) (Uemura and Kitagawa, 2003), polyethylenimine (PEI) (Zhai et al., 2008), polyaniline (PANI) (Zhang et al., 2007), and polyethylene glycol (PEG) (Hu et al., 2010). PVP, PEI and PANI all possess amide groups which can produce weak coordinate interactions with Fe ions. In the thermal environment, the rapidly formed PB crystals are fixed to the polymer chain instead of aggregated. Therefore, in this way, each newly formed crystal seed is uniformly distributed and slowly grows to a large size. As reported, well-defined nanocubic structures of PB with a highly homogeneous 50 nm size can be obtained under hydrothermal conditions with any one of the above amide-based polymers. In the absence of the amide group, PEG was able to accumulate PB nanoparticles at partial sites, which resulted in six square faces and eight truncated faces of a truncated cube (Zhang et al., 2007). With adjustment of PEG molecular weight, lower polymerized PEG is beneficial in the formation of much smaller and integrated mesocrystals. With a further decrease in the amount of PEG added, the nanostructure of synthesized PB shifted to a cube-like shape. Due to these findings, the authors claimed that PEG induced the mesocrystallization of PB.

Instead of polymers, Zheng et al. used glucose as the nanocrystallite stabilizer to obtain the regular cubic structure of PB powders (Zheng et al., 2007). Interestingly, some cubic crystals showed a large sized rectangular hole in the center (Fig. 4). By monitoring growth evolution,

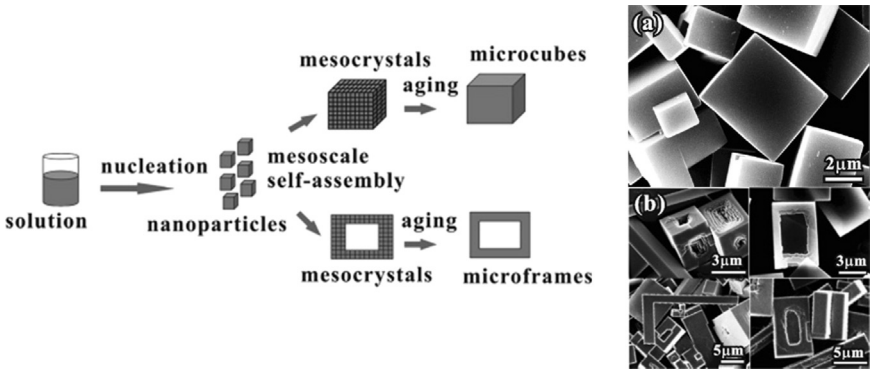

Fig. 4. Synthesis of PB microcubes and microframes by the hydrothermal method with glucose protection. Reproduced from Zheng et al. (2007) with permission from American Chemical Society.

the authors predicted a reasonable mechanism that, in a classic crystal growth, PB was inclined to shape the cubic structure. However, on the surface of the formed crystal, a CN group may be present, which would possibly react with the Fe ions released from the reactant $Fe(CN)_6^{3-}$ to fuse the boundaries of adjacent nanocrystallites. Therefore, the center of the cubic crystals was etched and showed a frame-like morphology.

However, without the addition of the above organic assistants, a direct hydrothermal process is also possible to create regular nanostructures of PB by controlling solution acidity and temperature (Hu et al., 2009). By employing $K_4[Fe(CN)_6]$ solution as the reactant, an octahedron shape of PB was crystallized, when 2 mol/L HCl was added at 120 °C for 24 h. The electron diffraction pattern shown by TEM suggested that although the octahedron morphology was complex, this PB crystal was still a single-crystal. The formation of this special mesostructure was attributed to the presence of H^+ cations from HCl. The authors explained that in the hot acid solution, dissociation of PB occurred easily and the already formed PB crystals were etched and reduced the nanoparticle concentration leading to oriented aggregation.

The hydrothermal process is good for regular nano- or microstructure crystal production. Its synthesis route is simple and the amount obtained is high. More importantly, with the change in various organic additives, different crystal morphologies can be obtained easily. However, for biosensor fabrication, this method does not realize *in-situ* crystal modification on the electrode surface due to the weak combination. Some researchers have introduced cross-linkers to adhere the prepared powders on the electrode for application. These extra sticky substances may cause blockage of the target reaction and electron transfer, which strongly affect the performance of the PB-based biosensors.

4.4. Other methods

In addition to the above-mentioned methods, special methods have been continuously developed for the control of PB nanostructures. These methods have not yet been widely used but possibly provide some inspiration for synthesis of the regular nanostructure of PB analogues and other materials.

The main problem in PB nanostructure formation is the fast crystallization rate. In terms of reaction kinetics, the classic equation for the reaction rate is described as follows (Laidler, 1979):

$$r = kc_A^{a_A} c_B^{a_B} \ldots = k \prod_{i=1}^{N} c_i^{a_i} \quad (2)$$

Where r is the reaction rate; a_A and a_B represent the reaction order of components A and B; C_A and C_B are the concentrations of reactants A and B; and k is the kinetic parameter of this reaction. According to the above principle, if the concentrations of the reactants can be greatly reduced during PB formation, only a small quantity of reactants will be needed to participate in the reaction, which will probably lead to a regular nanostructure. Therefore, we conceived an *in-situ* aerosol deposition route (Chu et al., 2010) to realize the slow formation of a nanostructured PB film. In this process, commonly employed $K_4[Fe(CN)_6]$ and $FeCl_3$ aqueous solutions were changed to aerosols which consisted of small units of reactants. When deposition time and temperature were controlled, well-defined PB nanocubes grew on the platinum surface, and the biosensing performance was increased two- or three-fold. Fig. 5.

Another method was introduced by Vaucher and colleagues (Vaucher et al., 2000), which was called the reverse microemulsion method. They used an anionic surfactant AOT, sodium bis(2-ethylhexyl)sulfosuccinate, for the preparation of reverse microemulsions to encapsulate the reactants $[Fe(C_2O_4)_3]^{3-}$ and $[Fe(CN)_6]^{3-}$ as the molecule shell to avoid the fast reaction of PB formation. The as-prepared microemulsions were kept stable in the dark at room temperature. However, after exposure to daylight, $[Fe(C_2O_4)_3]^{3-}$ was photoreduced to produce Fe^{2+}, which reacted with $[Fe(CN)_6]^{3-}$ to form nuclei and clusters of PB. Following further incubation, uniform PB nanocubes approximately 16 nm in size were obtained. Interestingly, the microemulsion medium was able to prevent the aggregation of already formed PB nanocubes. The size of the nanocubes only increased 2 or 4 nm after four days storage without any further protection strategy. This approach has provided a routine process for the preparation of ultrafine regular PB crystals.

Cao's group developed a sonochemical synthesis route for PB nanocubes from a single-source precursor (Wu et al., 2006). In this work, a very low concentration of 0.1 mM $K_4Fe(CN)_6$ was the only reactant with 0.1 M hydrochloric acid aqueous solution for preparation. Ultrasonic force was continuously applied to the precursor for 5 h, which also prolonged the PB formation time. The PB product showed a well-defined cubic structure with an approximate edge size of 250 nm. HRTEM demonstrated the formation of single crystalline to PB crystals and displayed the lattice fringes of the (200) and (020) crystal plane. All PB crystals were enclosed by its {100} facets. Accordingly, the authors proposed that the synthesis of a regular PB nanostructure relied on the slow dissociated Fe^{2+} ions from $K_4Fe(CN)_6$ in the acidic environment. The Fe^{2+} ion was rapidly oxidized to Fe^{3+}, and then reacted with the undecomposed $K_4Fe(CN)_6$ to form PB. The authors believed the ultrasonic effect contributed to cube formation, but no further results were provided.

Song et al. adopted a galvanic displacement method to synthesize PB nanoparticles (Song et al., 2007). $[Fe(CN)_6]^{3-}$ and Fe^{3+} ions in acidic solution were used as the reactants which did not directly induce the coordination reaction due to the lack of unshared paired electrons. In order to produce the reaction, they introduced a Si wafer to excite the galvanic displacement process. Due to the lower redox potential of the $Fe(CN)_6^{3-/4-}$ couple than the $Fe^{3+/2+}$ couple, $Fe(CN)_6^{3-}$ preferred to reduce when the valance electron was released from Si. The Si wafer surface was oxidized to SiO_2. Due to the presence of Fe^{3+} ions in solution, the PB film was immediately synthesized due to coordination between Fe^{3+} and $Fe(CN)_6^{4-}$ ions. The formed size and distributed density of PB particles was further demonstrated to be related to the concentration of Fe^{3+} and $Fe(CN)_6^{4-}$ ions. Round particles of 40 nm were the smallest obtained in this study. Furthermore, the authors used photolithographic techniques to map the PB patterns on the Si substrate, which exhibited high electrocatalysis for H_2O_2 detection.

Although these methods have not been widely used, they also confirm the possibility of further development of more advanced approaches in PB nanostructure control. Slowing down the reaction rate of PB is the key to realizing regular growth of PB crystals.

5. Applications of nanostructured PB biosensors

The first PB film-based biosensor was developed by Karyakin and coworkers in 1994 (Karyakin et al., 1994). They used an electrodeposition method to prepare a PB film for the electrocatalysis of glucose. Although various PB modified electrodes were subsequently widely fabricated, the nanostructure of PB film has not been elucidated. In the last ten years, the rapid progress in nanotechnology provides an opportunity for the promotion of PB film nanostructure control. Numerous advanced nanostructures have demonstrated their superior performance in the electrocatalysis of various physiological substances. Here, we have summarized the biosensors prepared using regular nanostructures of PB films in the recent literature, which are discussed in relation to the classification of different biosensing targets.

5.1. Detection of glucose

Glucose is one of the basic energy sources in living organisms (Liu et al., 2012a, 2012b; Qin et al., 2013). An abnormal glucose level often indicates diseases such as diabetes, liver and kidney damage (Shaw

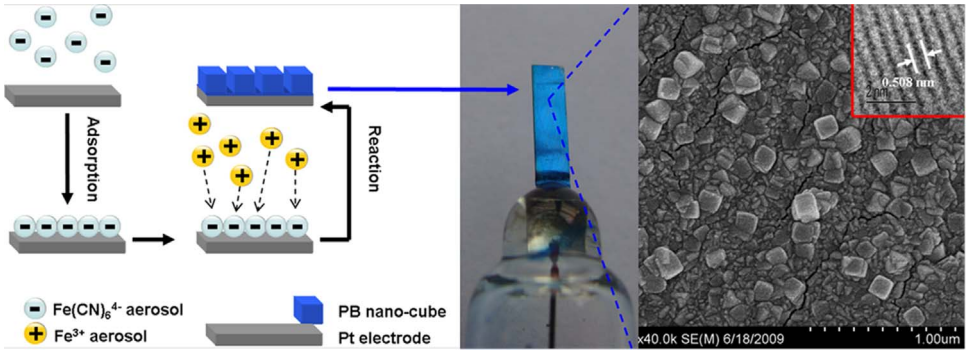

Fig. 5. Schematic of the aerosol deposition method for the *in-situ* fabrication of a PB nanocube-based electrode. Reproduced from Chu et al. (2010) with permission from Royal Society of Chemistry.

et al., 2005; Chen et al., 2016). Although commercial glucometers (Aziz and Hsiang, 1983; Xie et al., 2017) have been produced for the detection of blood sugar (glucose), many researchers are still investigating the development of novel glucose biosensors to enhance accuracy (Lai et al., 2016; Wang et al., 2016). Highly sensitive, selective and low-cost glucose biosensors are also continuously developed for research purposes (Liu et al., 2012a, 2012b). The biosensing process is mainly based on the following enzyme reaction (Liu et al., 2005; Lu et al., 2011):

$$\text{Glucose} + O_2 \xrightarrow[glucoseoxidase]{} Gluconolactone + H_2O_2 \quad (3)$$

It should be noted that glucose has two structures, D-glucose and L-glucose, distinguished by the positions of hydroxyls. Normally, only L-glucose can react with the oxidase, hence, freshly prepared glucose should be stored overnight for use.

Professor Wang classified all electrochemical glucose biosensors into three generations according to the different work principles (Wang, 2008). The first-generation glucose biosensor works due to natural oxygen in the solution. The second-generation glucose biosensor relies on the redox mediator for the electrocatalytic reaction and electron transfer. The third-generation glucose biosensor can directly transport the electrocatalytic electron from the active center of the enzyme (flavin adenine dinucleotide, FAD) to the electrode without a mediator. As previously mentioned, PB is an excellent electrocatalyst for H_2O_2. Therefore, the product of H_2O_2 from glucose oxidation can be directly reduced to produce electron transfer, which generates the current signal for detection. Most PB-based glucose biosensors follow the above electrocatalytic mechanism, and are classified as second-generation biosensors. The recent progress in biosensor performance is shown in Table 1. It should be noted that, in order to clarify the effects of the nanostructure on performance, only single PB material instead of the composite film-based biosensors are summarized. PB crystals have many morphologies, including nanocubes, nanowires, and nanoclusters, which have been synthesized for the fabrication of glucose biosensors. All listed biosensors can be operated under a low potential, normally < 0 V, which is beneficial for the promotion of anti-interference ability. As shown in Table 1, compared with irregular nanoparticles prepared by the traditional preparation methods, PB films composed of regular nanocrystals have superior performance in glucose sensing, especially sensitivity. The level of sensitivity is mainly determined by the electrocatalysis and conductivity of the applied material. Many reports have demonstrated that the crystals synthesized as regular shapes normally possess higher catalysis than irregular crystals due to increased active sites. However, we have not confirmed that the formation of regular PB morphology may enhance electron transfer resistance (Chu et al., 2010). However, the electrocatalysis of PB seems to dominate the performance. PB is a stable inorganic coordination compound with few active interaction sites; therefore, glucose oxidase (GOx) is normally immobilized by the cross-linkers. Glutaraldehyde (Yang et al., 2017), ionic liquid (Zhang et al., 2013), conductive polymers (Lai et al., 2016; Ramanavicius et al., 2017) and other functionalized materials (Karyakin, 2001; Lee et al., 2017) have been adopted for oxidase loading on PB films. Different cross-linkers can affect the performance of the enzyme reaction, which is often represented by the Michaelis-Menten constant (Dowd and Riggs, 1965) and shows the substrate's affinity for the enzyme. In addition, when the same cross-linker is used, Mattos et al. confirmed that different loading methods can also affect the performance of PB-based glucose biosensors (Mattos et al., 2001). These authors used Nafion dissolved in 90% ethanol as the cross-linker. Two different loading procedures were applied: (1) GOx and Nafion solutions were successively deposited on the PB film as two layers; (2) GOx and Nafion were previously mixed and deposited as one layer. According to their results, separate loading of GOx and the cross-linker showed much better sensitivity and stability. This may be attributed to the limited access of molecular oxygen in the film due to the GOx-nafion mixture.

5.2. Detection of lactate and glutamate

Lactate and glutamate are two important physiological indices in disease diagnosis. L-lactate is produced from pyruvate in the body by lactate dehydrogenase during metabolism and exercise (Chan et al., 2017). Its level can indicate tissue disease hypoxia, shock and respiratory failure (Coyle et al., 1983; Buckner et al., 2016). For detection by PB, lactate oxidase (LOx) is often employed in the following reaction (Stoisser et al., 2016):

$$\text{L} - \text{lactate} + O_2 \xrightarrow[lactateoxidase]{} Pyruvate + H_2O_2 \quad (4)$$

Glutamate is an essential excitatory neurotransmitter in cellular metabolism. Abnormal glutamate levels are mainly due to the occurrence of cerebral ischemia, Parkinson's disease and epilepsy (Coyle and Puttfarcken, 1993; Jenkins et al., 2016). In addition, its electrochemical detection often relies on its oxidase. The related enzyme reaction is as follows (Yao et al., 1990):

$$\text{L} - \text{glutamate} + O_2 + H_2O \xrightarrow[Glutamateoxidase]{} 2 - oxoglutarate + H_2O_2 \quad (5)$$

As shown in Eqs. (4) and (5), no matter which oxidase is selected, H_2O_2 is one of the most important products in the enzyme reaction. This is the basic requirement for the adoption of PB material as a biosensing film. Compared with glucose detection, fewer studies have focused on the preparation of lactate or glutamate biosensors (Table 1). Nanostructured PB films are rarely synthesized and used for the detection of lactate and glutamate. This may be attributed to the higher cost of lactate and glutamate oxidase. However, according to our research, the introduction of regular nanostructured PB can enhance the response current during electrocatalysis of lactate or glutamate, which is promising for decreasing the loading amount of oxidase and effectively reducing the cost. In addition, according to the performance outlined in Table 1, PB with a regular nanostructure synthesized by

Table 1
Applications of nanostructured PB biosensors in the literature.

Biosensing targets	Preparation methods	Nanostructure	Work potential (V)	Sensitivity (mA M^{-1} cm^{-2})	Limit of detection (μM)	Linear range (mM)	Reference
Glucose	Self-assembly	Nanocube	−0.05	127	10	0.01–1	Liu et al. (2014)
	Self-assembly	Nanogrid	−0.1	34.8	2	2×10^{-3}–1.5	Chu et al. (2012)
	Template-assisted method	Nanocube	−0.05	83.404	10	0.01–1.3	Jiang et al. (2016a, 2016b)
	Template-assisted method	Nanotube	−0.1	445	1	5×10^{-3}–8×10^{3}	Xian et al. (2007)
	Template-assisted method	Nanogrid	−0.1	30.63	10	0.01–1	Qiu et al. (2007a, 2007b)
	Hydrothermal method	Nanocube	0	46.7	5	1.6×10^{-2}–8.5	Wang et al. (2013)
	Aerosol deposition	Nanocube	−0.05	359	10	0.01–1	Xu et al. (2015)
	Chemical reaction method	Irregular nanoparticle	−0.05	2	7	0.02–0.4	Du et al. (2010)
	Electrochemical deposition method	Irregular nanoparticle	0.05	1.9	–	0.1–20	Ramanavicius et al. (2017)
Lactate	Self-assembly	Nanocube	−0.05	12.5	10	0.01–0.1	Liu et al. (2014)
	Self-assembly	Nanogrid	−0.1	4.5	10	0.01–2.4	Chu et al. (2012)
	Template-assisted method	Nanocube	−0.05	6.379	10	0.01–0.5	Jiang et al. (2016a, 2016b)
	Chemical reaction method	–	−0.1	0.096	–	0–28	Imani et al. (2016)
	Electrochemical deposition method	Irregular nanoparticle	−0.1	1.36	0.84	4.4×10^{-3}–2.24	Lowinsohn and Bertotti (2007)
	Self-assembly	Nanocube	−0.05	238	10	0.01–0.1	Liu et al. (2014)
Glutamate	Self-assembly	Nanogrid	−0.1	12.36	10	0.01–1.2	Chu et al. (2012)
	Template-assisted method	Nanocube	−0.05	31.642	10	0.01–1	D Jiang et al. (2016); Y Jiang et al. (2016)
	Electrochemical deposition method	Irregular nanoparticle	0	210	0.1	10^{-4}–10^{-1}	Karyakin et al. (2000)
	Electrochemical deposition method	Irregular nanoparticle	0	0.13	1.5	1.5×10^{-3}–0.15	Salazar et al. (2016)

novel developed methods shows higher sensitivity in the detection of lactate and glutamate, which is consistent with glucose analysis. Therefore, the design of more advanced PB nanostructures with high electrocatalysis of lactate and glutamate is meaningful for the further development of industrial biosensor devices.

In addition, PB nanostructured films have also been used in the detection of choline (Keihan et al., 2014), L-cysteine (Pandey et al., 2012), organophosphorus pesticides (Zhao et al., 2015) and xanthine (Harrad et al., 2016). The enhancement of performance due to the PB nanostructure has been confirmed, although the related research has not been widely extended. It is expected that, with better recognition of PB crystallization behavior, more and different nanostructures of PB will be developed for future potential applications.

6. Conclusions and perspectives

We have summarized the main synthesis methods of nanostructured PB films, with special emphasis on novel techniques for regular nanostructure control. The mechanisms of these methods for regular PB crystallization are discussed, and a general rule for the design of novel synthesis approaches for regular PB nanostructure control has been proposed. Overall, in order to obtain the regular shape of PB crystals, a slow kinetic reaction rate is required, and certain protectors should be adopted to decrease aggregation of the formed crystals. These regular nanostructures of PB have been confirmed to possess superior electrocatalysis to enhance biosensing performance. This is mainly due to more active sites provided by the regular crystal shape for electrocatalysis.

Not only PB, but also PB analogues rely on the same reaction between the metal cation and metal cyanide anion for synthesis. Therefore, all mentioned approaches in this review are also expected to apply to the synthesis of regular nanostructures of PB analogues. PB analogues have already been adopted in biosensor fabrication, and some results have confirmed their superior performance. Currently, PB and its analogues are also used in other important fields, such as fuel cells, gas separation and environmental monitoring. However, in these fields, nanostructured PB has not been widely adopted. We believe that, with the development of more advanced nanostructures of PB and its analogues, this stable coordination compound can be further developed in various scientific areas.

Acknowledgement

This work was financially supported by the Innovative Research Team Program by the Ministry of Education of China (No. IRT13070), the National Natural Science Foundation of China (No. 21490585, 21476107, 21406107), the Jiangsu Province Natural Science Foundation for the Youth (No. BK20140931) and Top-notch Academic Programs Project of Jiangsu Higher Education Institutions (TAPP).

References

Abbaspour, A., Kamyabi, M., 2005. J. Electroanal. Chem. 584, 117–123.
Aguila, D., Prado, Y., Koumousi, E.S., Mathoniere, C., Clerac, R., 2016. Chem. Soc. Rev. 45, 203–224.
Aziz, S., Hsiang, Y.H., 1983. Diabetes Care 6, 529–532.
Bleuzen, A., Escax, V., Ferrier, A., Villain, F., Verdaguer, M., Munsch, P., Itie, J., 2004. Angew. Chem. Int. Ed. 43, 3728–3731.
Buckner, S., Loenneke, J., Loprinzi, P., 2016. Sprots Med. 46, 467–472.
Buser, H.J., Schwarzenbach, D., Petter, W., Ludi, A., 1977. Inorg. Chem. 16, 2704–2710.
Chan, D., Barsan, M., Korpan, Y., Brett, C., 2017. Electrochim. Acta 231, 209–215.
Chen, T., Liu, D., Lu, W., Wang, K., Du, G., Asiri, A., Sun, X., 2016. Anal. Chem. 88, 7885–7889.
Chu, Z., Zhang, Y., Dong, X., Jin, W., Xu, N., Tieke, B., 2010. J. Mater. Chem. 20, 7815–7820.
Chu, Z., Shi, L., Zhang, Y., Jin, W., Xu, N., 2011. J. Mater. Chem. 21, 11968–11972.
Chu, Z., Shi, L., Zhang, Y., Jin, W., Warren, S., Ward, D., Dempsey, E., 2012. J. Mater. Chem. 22, 14874–14879.
Coleby, L.J.M., 1939. Ann. Sci. 4, 206–211.
Coyle, E.F., Martin, W.H., Ehsani, A.A., Hagberg, J.M., Bloomfield, S.A., Sinacore, D.R., Holloszt, J.O., 1983. J. Appl. Physiol. 54, 18–23.
Coyle, J.T., Puttfarcken, P., 1993. Science 262, 689–695.
Crumbliss, A.L., Lugg, P.S., Morosoff, N., 1984. Inorg. Chem. 23, 4701–4708.
DeLongchamp, D.M., Hammond, P.T., 2004. Chem. Mater. 16, 4799–4805.
Doumic, L.I., Salierno, G., Ramos, C., Haure, P.M., Cassanello, M.C., Ayude, M.A., 2016. RSC Adv. 6, 46625–46633.
Dowd, J.E., Riggs, D.S., 1965. J. Biol. Chem. 240, 863–869.
Du, J., Wang, Y., Zhou, X., Xue, Z., Liu, X., Sun, K., Lu, X., 2010. J. Phys. Chem. C 114, 14786–14793.

Du, X., Hao, X., Wang, Z., Guan, G., 2016. J. Mater. Chem. A 4, 6236–6258.
Ellis, D., Eckhoff, M., Neff, V.D., 1981. J. Phys. Chem. 85, 1225–1231.
Ferlay, S., Mallah, T., Ouahes, R., Veillet, P., Verdaguer, M., 1995. Nature 378, 701–703.
Gao, Z., Qu, Y., Li, T., Shrestha, N.K., Song, Y., 2014. Sci. Rep. 4, 6891.
Gimenez-Romero, D., Agrisuelas, J., Garcia-Jareno, J., Gregori, J., Gabrielli, C., Perrot, H., Vicente, F., 2007. J. Am. Chem. Soc. 129, 7121–7126.
Goux, A., Ghanbaja, J., Walcarius, A., 2009. J. Mater. Sci. 44, 6601–6607.
Guo, Y., Guadalupe, A.R., Resto, O., Fonseca, L.F., Weisz, S.Z., 1999. Chem. Mater. 11, 135–140.
Haghighi, B., Hamidi, H., Gorton, L., 2010. Sens. Actuators B: Chem. 147, 270–276.
Han, L., Yu, X., Lou, X., 2016. Adv. Mater. 28, 4601–4605.
Harrad, L., Amine, A., 2016. Enzym. Microb. Tech. 85, 57–63.
Herren, F., Fischer, P., Ludi, A., Haelg, W., 1980. Inorg. Chem. 19, 956–959.
Holtzman, H., 1945. Ind. Eng. Chem. 37, 855–861.
Hu, M., Jiang, J., Ji, R., Zeng, Y., 2009. Cryst. Eng. Comm. 11, 2257–2259.
Hu, M., Jiang, J., Lin, C., Zeng, Y., 2010. Cryst. Eng. Comm. 12, 2679–2683.
Imani, S., Bandodkar, A.J., Mohan, A.M.V., Kumer, R., Yu, S., Wang, J., Mercier, P.P., 2016. Nat. Commun. 7, 11650.
Itaya, K., Shibayama, K., Akahoshi, H., Toshima, S., 1982. J. Appl. Phys. 53, 804–805.
Itaya, K., Uchida, I., Neff, V.D., 1986. Acc. Chem. Res. 19, 162–168.
Jenkins, B., Zhu, A., Poutiainen, P., Choi, J., Kil, K., Zhang, Z., Kuruppu, D., Aytan, N., Dedeoglu, A., Brownell, A., 2016. Neuropharmacology 108, 462–473.
Jiang, D., Chu, Z., Peng, J., Jin, W., 2016. Sens. Actuators B: Chem. 228, 679–687.
Jiang, Y., Yu, S., Wang, B., Li, Y., Sun, W., Lu, Y., Yan, M., Song, B., Dou, S., 2016. Adv. Funct. Mater. 26, 5315–5321.
Johansson, A., Widenkvist, E., Lu, J., Boman, M., Jansson, U., 2005. Nano Lett. 5, 1603–1606.
Karyakin, A., Karyakina, E., Gorton, L., 1999. Electrochem. Commun. 1, 78–82.
Karyakin, A., Puganova, E., Bolshakov, I., Karyakina, E., 2007. Angew. Chem. Int. Ed. 46, 7678–7680.
Karyakin, A.A., 2001. Electroanalysis 13, 813–819.
Karyakin, A.A., Gitelmacher, O.V., Karyakina, E.E., 1994. Anal. Lett. 27, 2861–2869.
Karyakin, A.A., Gitelmacher, O.V., Karyakina, E.E., 1995. Anal. Chem. 67, 2419–2423.
Karyakin, A.A., Karyakina, E.E., Gorton, L., 2000. Anal. Chem. 72, 1720–1723.
Kaye, S.S., Long, J.R., 2005. J. Am. Chem. Soc. 127, 6506–6507.
Keihan, A., Sajjadi, S., Sheibani, N., Movahedi, A., 2014. Sens. Actuators B: Chem. 204, 684–703.
Lai, J., Yi, Y., Zhu, P., Shen, J., Wu, K., Zhang, L., Liu, J., 2016. J. Electroanal. Chem. 782, 138–153.
Laidler, K.J., 1979. Theories of Chemical Reaction Rates. R. E. Krieger Pub. Co., Michigan, USA.
Lee, H., Song, C., Hong, Y., Kim, M., Cho, H., Kang, T., Shin, K., Choi, S., Hyeon, T., Kim, D., 2017. Sci. Adv. 3, 1–8.
Lee, W., Park, S., 2014. Chem. Rev. 114, 7487–7556.
Li, Y., Duan, G., Liu, G., Cai, W., 2013. Chem. Soc. Rev. 42, 3614–3627.
Liu, L., Shi, L., Chu, Z., Peng, J., Jin, W., 2014. Sens. Actuators B: Chem. 202, 820–826.
Liu, S., Tian, J., Wang, L., Qin, X., Zhang, Y., Luo, Y., Asiri, A., Al-Youbi, A., Sun, X., 2012a. Catal. Sci. Technol. 2, 813–817.
Liu, S., Tian, J., Wang, L., Luo, Y., Sun, X., 2012b. RSC Adv. 2, 411–413.
Liu, Y., Wang, M., Zhao, F., Xu, Z., Dong, S., 2005. Biosens. Bioelectron. 21, 984–988.
Liu, Y., Chu, Z., Jin, W., 2009a. Electrochem. Commun. 11, 484–487.
Liu, Y., Chu, Z., Zhang, Y., Jin, W., 2009b. Electrochim. Acta 54, 7490–7494.
Lowinsohn, D., Bertotti, M., 2007. Anal. Biochem. 365, 260–265.
Lu, W., Luo, Y., Chang, G., Sun, X., 2011. Biosens. Bioelectron. 26, 4791–4797.
Lu, X., Nan, Z., Qiu, Y., Zheng, L., Lu, X., 2013. Electrochim. Acta 90, 203–209.
Lu, Y., Wang, L., Cheng, J., Goodenough, J.B., 2012. Chem. Commun. 48, 6544–6546.
Manivannan, S., Kang, I., Kim, K., 2016. Langmuir 32, 1890–1898.
Mattos, I., Lukachova, L., Gorton, L., Laurell, T., Karyakin, A.A., 2001. Talanta 54, 963–974.
McHale, R., Ghasdian, N., Liu, Y., Ward, M.B., Honow, N.S., Wang, H., Miao, Y., Brydson, R., Wang, X., 2010. Chem. Commun. 46, 4574–4576.
Millward, R.C., Madden, C.E., Sutherland, I., Mortimer, R.J., Fletcher, S., Marken, F., 2001. Chem. Commun., 1994–1995.
Mo, M., Zeng, J., Liu, X., Yu, W., Zhang, S., Qian, Y., 2002. Adv. Mater. 14, 1658–1662.
Murray, R.W., 1980. Acc. Chem. Res. 13, 135–141.
Neff, V.D., 1978. J. Electrochem. Soc. 125, 886–887.
Okubo, M., Asakura, D., Mizuno, Y., Kim, J.D., Mizokawa, T., Kudo, T., Honma, I., 2010. J. Phys. Chem. Lett. 1, 2063–2071.
Pandey, P.C., Pandey, A.K., Chauhan, D.S., 2012. Electrochim. Acta 74, 23–31.
Puganova, E.A., Karyakin, A.A., 2005. Sens. Actuators B: Chem. 109, 167–170.
Qin, X., Lu, W., Asiri, A., Al-Youbim, A., Sun, X., 2013. Catal. Sci. Technol. 3, 1027–1035.
Qiu, J., Peng, H., Liang, R., Li, J., Xia, X., 2007a. Langmuir 23, 2133–2137.
Qiu, J., Peng, H., Liang, R., Xiong, M., 2007b. Electroanalysis 19, 1201–1206.
Qu, F., Shi, A., Yang, M., Jiang, J., Shen, G., Yu, R., 2007. Anal. Chim. Acta 605, 28–33.
Ramanavicius, A., Rekertaite, A., Valiunas, R., Valiuniene, A., 2017. Sens. Actuators B: Chem. 240, 220–223.
Ricci, F., Palleschi, G., 2005. Biosens. Bioelectron. 21, 389–407.
Ricci, F., Amine, A., Palleschi, G., Moscone, D., 2003. Biosens. Bioelectrons. 18, 165–174.
Routkevitch, D., Bigioni, T., Moskovits, M., Xu, J., 1996. J. Phys. Chem. 100, 14037–14047.
Roy, X., Hui, J., Rabnawaz, M., Liu, G., Lachlan, M., 2011. Angew. Chem. Int. Ed. 50, 1597–1602.
Salazar, P., Martin, M., O'Neill, R.D., Gonzalez-Mora, J.L., 2016. Sens. Actuators B: Chem. 235, 117–125.
Sgobbi, L.F., Razzino, C.A., Machado, S.A.S., 2016. Electrochim. Acta 191, 1010–1017.
Shaw, R.J., Lamia, K.A., Vasquez, D., Koo, S., Bardeesy, N., Depinho, R.A., Montminy, M., Cantley, L.C., 2005. Science 310, 1642–1646.
Shen, Q., Jiang, J., Fan, M., Liu, S., Wang, L., Fan, Q., Huang, W., 2014. J. Electroanal. Chem. 712, 132–138.
Shen, X., Wu, S., Liu, Y., Wang, K., Xu, Z., Liu, W., 2009. J. Colloid Interf. Sci. 329, 188–195.
Song, Y., Jia, W., Li, Y., Xia, X., Wang, Q., Zhao, J., Yan, Y., 2007. Adv. Funct. Mater. 17, 2808–2814.
Stoisser, T., Brunsteiner, M., Wilson, D., Nidetzky, B., 2016. Sci. Rep. 6, 27892.
Tang, H., Chu, Z., Li, C., Ren, X., Xue, C., Jin, W., 2016. Dalton Trans. 45, 10249–10255.
Thomas, A., Goettmann, F., Antonietti, M., 2008. Chem. Mater. 20, 738–755.
Uemura, T., Kitagawa, S., 2003. J. Am. Chem. Soc. 125, 7814–7815.
Vaucher, S., Li, M., Mann, S., 2000. Angew. Chem. Int. Ed. 39, 1793–1796.
Wang, J., 2008. Chem. Rev. 108, 814–825.
Wang, L., Ye, Y., Lu, X., Wu, Y., Sun, L., Tan, H., Xu, F., Song, Y., 2013. Electrochim. Acta 114, 223–232.
Wang, X., Li, Y., 2002a. J. Am. Chem. Soc. 124, 2880–2881.
Wang, X., Li, Y., 2002b. Angew. Chem. Int. Ed. 41, 4790–4793.
Wang, Y., Angelatos, A.S., Caruso, F., 2008. Chem. Mater. 20, 848–858.
Wang, Z., Cao, X., Liu, D., Hao, S., Du, G., Asiri, A., Sun, X., 2016. Chem. Commun. 52, 14438–14441.
Ware, M., 2008. J. Chem. Educ. 85, 612.
Wu, X., Cao, M., Hu, C., He, X., 2006. Cryst. Growth Des. 6, 26–28.
Xian, Y., Hu, Y., Liu, F., Xian, Y., Feng, L., Jin, L., 2007. Biosens. Bioelectron. 22, 2827–2833.
Xiao, C., Chu, Z., Ren, X., Chen, T., Jin, W., 2015. Chem. Commun. 51, 7947–7949.
Xie, L., Asiri, A., Sun, X., 2017. Sens. Actuators B: Chem. 244, 11–16.
Xu, H., Wang, W., 2007. Angew. Chem. Int. Ed. 46, 1489–1492.
Xu, Y., Chu, Z., Shi, L., Peng, J., Jin, W., 2015. Sens. Actuators B: Chem. 221, 1009–1016.
Yamamoto, T., Saso, N., Umemura, Y., Einaga, Y., 2009. J. Am. Chem. Soc. 131, 13196–13197.
Yang, P., Peng, J., Chu, Z., Jiang, D., Jin, W., 2017. Biosens. Bioelectron. 92, 709–717.
Yao, T., Kobayashi, N., Wasa, T., 1990. Anal. Chim. Acta 231, 121–124.
Yu, X., Wang, H., Liu, Y., Zhou, X., Li, B., Xin, L., Zhou, Y., Shen, H., 2013. J. Mater. Chem. A 1, 2110–2117.
Zakharchuk, N.F., Meyer, B., Henning, H., Scholz, F., Jaworksi, A., Stojek, Z., 1995. J. Electroanal. Chem. 398, 23–35.
Zhai, J., Zhai, Y., Wang, L., Dong, S., 2008. Inorg. Chem. 47, 7071–7073.
Zhang, D., Zhang, K., Yao, Y., Xia, X., Chen, H., 2004. Langmuir 20, 7303–7307.
Zhang, W., Hu, S., Yin, J., He, W., Lu, W., Ma, M., Gu, N., Zhang, Y., 2016. J. Am. Chem. Soc. 138, 5860–5865.
Zhang, X., Sui, C., Gong, J., Yang, R., Luo, Y., Qu, L., 2007. Appl. Surf. Sci. 253, 9030–9034.
Zhang, Y., Wen, Y., Liu, Y., Li, D., Li, J., 2004. Electrochem. Commun. 6, 1180–1184.
Zhang, Y., Chu, Z., Shi, L., Jin, W., 2011. Electrochim. Acta 56, 8163–8167.
Zhang, Y., Liu, Y., Chu, Z., Shi, L., Jin, W., 2013. Sens. Actuators B: Chem. 176, 978–984.
Zhao, H., Ji, X., Wang, B., Wang, N., Li, X., Ni, R., Ren, J., 2015. Biosens. Bioelectron. 65, 23–30.
Zhao, W., Xu, J., Shi, C., Chen, H., 2005. Langmuir 21, 9630–9634.
Zheng, X., Kuang, Q., Xu, T., Jiang, Z., Zhang, S., Xie, Z., Huang, R., Zheng, L., 2007. J. Phys. Chem. C 111, 4499–4502.
Zhou, P., Xue, D., Luo, H., Chen, X., 2002. Nano Lett. 2, 845–847.